First-principles study of the dielectric and dynamical properties of lithium niobate

M. Veithen and Ph. Ghosez
Département de Physique, Université de Liège, B-5, B-4000 Sart-Tilman, Belgium
(Received 6 November 2001; revised manuscript received 18 January 2002; published 20 May 2002)

Using a first-principles approach based on density-functional theory, the electronic, dielectric, and dynamical properties of the two phases of lithium niobate are studied. In particular, the spontaneous polarization, the optical dielectric tensors, the Born effective charges, and the zone-center phonons are computed. The Born effective charges are found to be significantly larger than the nominal ionic charges of the ions, a feature similar to what is observed in related ABO_3 compounds and attributed to the hybridization between the O $2p$ and Nb $4d$ states. The analysis of the zone-center phonons in the paraelectric phase reveals an unstable A_{2u} mode to be responsible for the phase transition. The origin of the structural instability is attributed to destabilizing long-range dipolar interactions, which are not fully compensated by stabilizing short-range forces. Finally, the identification of the E modes in the ferroelectric phase, which is still the cause for debates in spite of the numerous experimental and theoretical studies, is discussed and an assignation based on the analysis of the mode-oscillator strengths and the angular dispersion relation of extraordinary phonons is proposed.

DOI: 10.1103/PhysRevB.65.214302 PACS number(s): 63.20.−e, 77.84.−s, 31.15.Ar

I. INTRODUCTION

Lithium niobate ($LiNbO_3$) belongs to the class of ferroelectric oxides. Its good electro-optic, photorefractive, and nonlinear optical properties make it nowadays a widely used material in devices such as modulators for fiber-optic communications systems[1–3] or holographic applications.[4,5]

Many ABO_3 coumpounds such as $BaTiO_3$ have a perovskite structure.[1] In contrast, lithium niobate has two phases of trigonal symmetry with ten atoms per unit cell: a high-symmetric paraelectric phase (space group $R\bar{3}c$) stable above 1480 K and a ferroelectric ground state (space group $R3c$). Because of its high transition temperature T_c and due to the fact that its melting point (about 1520 K) is quite close to T_c, only few experimental data are available on the paraelectric phase. On the contrary, during the last decades, the ferroelectric phase has been the subject of numerous experimental and theoretical studies.

A good review that summarizes a wide range of experimental results is proposed in Ref. 6. From a theoretical point of view, a few first-principles studies have been performed. Without being exhaustive, let us cite the papers of Inbar and Cohen,[7,8] who identified the nature of the phase transition to be mainly of the order-disorder type. More recently, Caciuc and co-workers[9,10] have calculated zone-center phonons in the ferroelectric phase, and Parlinski, Li, and Kawawzoe[11] have obtained phonon-dispersion relations in the two phases.

The present work is intended to complete the set of existing data on lithium niobate. In particular, we report the Born effective charges and the optical dielectric tensors in the two phases. The knowledge of these quantities allows us to deduce the frequencies of the longitudinal phonon modes at the Γ point and to investigate the origin of the ferroelectric instability. We also pay particular attention to the assignation of the E phonon modes in the ferroelectric phase. We draw several comparisons with the perovskites and show that, in spite of its different structure, $LiNbO_3$ has a very similar behavior. Beside using the local-density approximation (LDA), as was the case in the previous works cited above, we also compute some properties within a generalized gradient approximation (GGA) for the exchange-correlation energy. This allows to compare the results and to examine the impact of both kinds of approximations.

Our paper is organized as follows. Using a first-principles density-functional approach, we first study ground-state properties (Sec. III) such as the atomic and electronic structures and the spontaneous polarization appearing during the phase transition. We then discuss dielectric properties (Sec. IV) such as the optical dielectric tensor and the Born effective charges. We finally report the phonons at the Γ point (Sec. V) in the two phases and deduce the static dielectric tensor for the ferroelectric phase.

II. METHOD

Our calculations were performed in the framework of the density-functional theory (DFT), as was developed by Hohenberg, Kohn, and Sham.[12,13] We used the ABINIT package,[14] a plane-wave pseudopotential DFT code, which, in addition to usual ground-state calculations allows linear-response computations of the phonon frequencies, Born effective charges, and dielectric constants.[15,16] It relies on an efficient fast Fourier transform algorithm[17] for the conversion of wave functions between real and reciprocal space, on the adaptation to a fixed potential of the band-by-band conjugate-gradient method,[18] and on a potential-based conjugate-gradient algorithm for the determination of the self-consistent potential.[19]

For the exchange-correlation functional, we chose either the LDA as parametrized by Perdew and Wang[20] or the GGA proposed by Perdew, Burke, and Ernzerhof.[21] The all-electron potentials were replaced by norm-conserving pseudopotentials generated according to the Troullier-Martins scheme[22] thanks to a package developed at the Fritz-Haber Institute, Berlin.[23] Niobium $4s$, $4p$, $4d$, and $5s$ electrons, lithium $1s$ and $2s$ electrons, as well as oxygen $2s$ and $2p$ electrons were considered as valence states in the con-

struction of the pseudopotentials.

For the calculations within the LDA, the wave functions were expanded in plane waves up to a kinetic-energy cutoff of 45 hartree and the Brillouin zone was sampled using a $6\times6\times6$ Monkhorst-Pack[24] mesh of special k points. These parameters were necessary to obtain converged results in the linear-response calculations of phonon frequencies and Born effective charges. A 35 hartree cutoff and a $4\times4\times4$ grid of special k points were already enough to obtain converged values for the lattice constants and atomic positions and were used in the GGA determination of these quantities.

III. GROUND-STATE PROPERTIES

A. Structural data

As a first step, we determined the structural parameters of lithium niobate in its two phases by relaxing simultaneously the cell shape and the atomic positions. In the optimized structures reported here, the forces on the atoms are less than 10^{-5} hartree/bohr and the stresses on the unit cell are smaller than 10^{-7} hartree/bohr^3. The two phases of $LiNbO_3$ are rhombohedral with ten atoms in the unit cell. To describe their geometry, one can either use the primitive (rhombohedral) or an hexagonal unit cell. In the discussion of our results, the symbols a and c correspond to the lengths of the basis vectors of the hexagonal unit cell. Atomic positions are given in hexagonal coordinates.

The paraelectric phase belongs to the space group $R\bar{3}c$. The positions of the ten atoms in the rhombohedral unit cell are shown on Fig. 1. The threefold axis is formed by a chain of equidistant niobium and lithium atoms. Each niobium is located at the center of an octaedron formed by six oxygen atoms. In Table I, we define the parameters that determine the atomic positions in the two phases by reporting the hexagonal coordinates of five atoms of the rhombohedral unit cell. The coordinates of the other atoms can easily be obtained by using the symmetry operations of the space groups $R\bar{3}c$ and $R3c$.

In the paraelectric phase, the positions of the niobium and lithium atoms are fixed by symmetry, while the positions of the oxygen atoms are determined by the internal parameter x. The results of our structural optimizations are summarized in Table II. They are compared to the results obtained by Parlinski *et al.*[11] and Postnikov *et al.*[9] as well as to the experimental data deduced from neutron diffraction on a powder.[25] The GGA gives the closest agreement with experiment, whereas our LDA results present errors similar to those of the previous DFT calculations (also performed within the LDA).

The ferroelectric phase belongs to the space group $R3c$. During the structural optimizations, we held the niobium Nb_1 atom fixed at the origin. The coordinates of the lithium and oxygen atoms are reported in the lower part of Table I. Our results for the ferroelectric phase are summarized in Table III. As for the paraelectric phase, our values are close to those of Parlinski *et al.*[11] Again, we tried to improve the accuracy of the calculation using the GGA. However, this does not yield a significative improvement: looking, for example, at the value of the parameter a, we observe that the GGA tends to overcorrect the errors of the LDA, a fact already observed in this kind of calculations.[26,27]

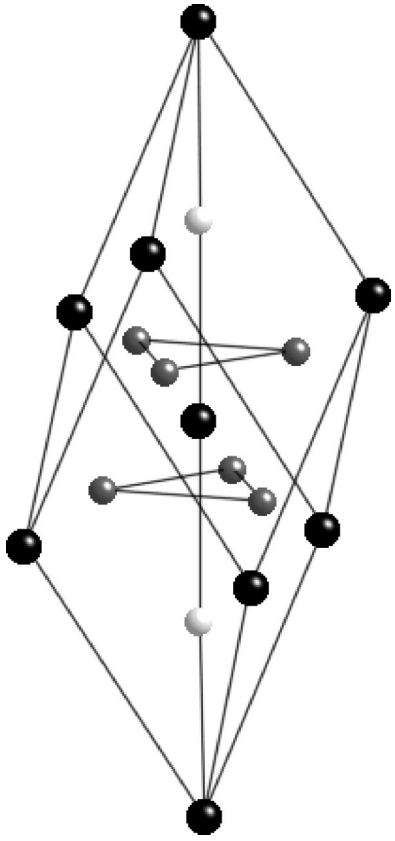

FIG. 1. Primitive unit cell of the paraelectric phase of $LiNbO_3$.

Comparing Tables II and III, we see that our values for the lattice parameters are in better agreement with the experiment for the ferroelectric than for the paraelectric phase. A possible explanation is that we determined the ground state of the compound at 0 K and we thus neglected the effects of the thermal expansion. As the paraelectric phase of lithium niobate is only stable above 1480 K, these effects are more

TABLE I. Atomic positions (in hexagonal coordinates) in the two phases of litihium niobate.

Phase	Atom	Position
Paraelectric	Nb_1	$(0,0,0)$
	Li_1	$(0,0,\frac{1}{4})$
	O_1	$(-\frac{1}{3},-\frac{1}{3}+x,\frac{7}{12})$
	O_2	$(\frac{1}{3}-x,-x,\frac{7}{12})$
	O_3	$(x,\frac{1}{3},\frac{7}{12})$
Ferroelectric	Nb_1	$(0,0,0)$
	Li_1	$(0,0,\frac{1}{4}+z)$
	O_1	$(-\frac{1}{3}-u,-\frac{1}{3}+v,\frac{7}{12}-w)$
	O_2	$(\frac{1}{3}-v,-u-v,\frac{7}{12}-w)$
	O_3	$(u+v,\frac{1}{3}+u,\frac{7}{12}-w)$

TABLE II. Lattice constants and atomic position parameter x (see Table I) in the paraelectric phase of lithium niobate.

	a (Å)	c (Å)	x
Expt. (Ref. 25)	5.289	13.848	0.060
Calc. (LDA) (Ref. 9)	5.138	13.499	0.049
Calc. (LDA) (Ref. 11)	5.097	13.708	0.036
Present (LDA)	5.125	13.548	0.042
Present (GGA)	5.255	13.791	0.048

important for this phase than for the ferroelectric one and the calculated parameters tend to be smaller than the measured ones.

B. Electronic properties

In Fig. 2, we report the Kohn-Sham band structure of the paraelectric phase of lithium niobate obtained within the LDA. The notations of the high-symmetry points between which we have drawn the band structure correspond to those chosen in Ref. 28. We observe the presence of well-separated groups of bands. Each of these groups has a marked dominant character and has been labeled by the name of the atomic orbital that mainly composes this energy state in the solid.

As previously discussed by Inbar and Cohen,[7,8] the chemical bonding in lithium niobate has a mixed covalent-ionic character. The Nb $4d$ and O $2p$ atomic orbitals strongly interact to form the valence and conduction bands near the Fermi level, while the Li atoms completely loose their $2s$ electrons. In other words, the bonding between niobium and oxygen atoms has a non-negligible covalent character, while the bonding with the lithium atoms is essentially ionic. This mixed feature is similar to what has been observed in most perovskite ABO_3 compounds such as $KNbO_3$ and $BaTiO_3$ (Ref. 29) but different from the case of $PbTiO_3$,[30–32] in which the lead atom has a covalent interaction with the oxygen.

The transition to the ferroelectric state mainly affects the bands in the region close to the Fermi level. In LDA the indirect band gap E_g increases from 2.60 to 3.48 eV and the spread of the O $2p$ bands reduces from 5.06 to 4.71 eV. In GGA, we obtained similar values for E_g (2.51 and 3.50 eV), while the O $2p$ group is narrower than in LDA in both the paraelectric (4.80 eV) and the ferroelectric phase (4.48 eV). We note that, in spite of the well-known DFT band gap problem,[33] the values of E_g in the ferroelectric phase only slightly underestimate the experimental value of 3.78 eV.[34] For the deeper bands, the spread remains unaffected at the transition while the position with respect to the top of the valence band is slightly shifted to higher energies. We conclude that the only significant effect of the phase transition on the electronic properties is to modify the hybridizations between O $2p$ and Nb $4d$ orbitals.

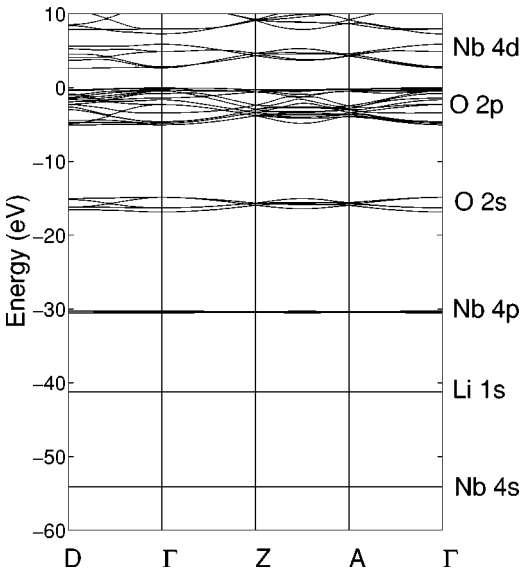

FIG. 2. Kohn-Sham electronic band structure in the paraelectric phase of $LiNbO_3$ calculated within the LDA.

C. Spontaneous polarization

The modern theory of polarization, as was developed by Resta,[35] and King-Smith and Vanderbilt,[36,37] identifies the spontaneous polarization of a ferroelectric material to a Zak phase of the electronic wave functions. We used this approach to calculate the spontaneous polarization of lithium niobate.

The formulas we used are described in Ref. 36 [in particular, Eq. (16)]. To calculate the polarization, we sampled the Brillouin zone by a $4\times4\times20$ mesh of k points. We calculated the polarization for the two phases of $LiNbO_3$ and then took the difference to get the spontaneous polarization. Our results, obtained in the LDA and GGA, are summarized in Table IV. We compare them to experimental values obtained by a field reversal method[38] and a pyroelectric measurement.[39] For completeness, we also mention a value

TABLE III. Lattice constants and atomic position parameters (see notations of Table I) in the ferroelectric phase of lithium niobate.

	a (Å)	c (Å)	z	u	v	w
Expt. (Ref. 25)	5.151	13.876	0.0329	0.00947	0.0383	0.0192
Calc. (LDA) (Ref. 11)	5.086	13.723	0.0350	0.01497	0.0247	0.0186
Present (LDA)	5.067	13.721	0.0337	0.01250	0.0302	0.0183
Present (GGA)	5.200	13.873	0.0318	0.00973	0.0382	0.0199

TABLE IV. Spontaneous polarization of lithium niobate.

	P_s (C/m^2)
Expt. (Ref. 38)	0.71
Expt. (Ref. 39)	0.70
Calc. (Ref. 40)	0.77
LDA	0.80
GGA	0.80

reported by Hafid and Michel-Calendini,[40] even if their calculation was conceptually wrong in the sense that it was making use of static charges deduced from a population analysis of the $X\alpha$ electronic distribution of a NbO_6 cluster, instead of the dynamical Born effective charges (see Sec. IV B).

Our values overestimate the experimental results by 0.1 C/m^2. This agreement is not perfect, but comparable to what has been obtained in perovskite ferroelectrics.[41] Part of the error could be assigned to the use of DFT and approximate functionals.[42] Another origin for the error could be attributed to the fact that our calculated value is an upper limit, related to an idealized perfect crystal. A real sample always presents defects that tend to lower the measured polarization.

IV. DIELECTRIC PROPERTIES

A. The optical dielectric tensor

We have calculated the optical dielectric permitivity tensors $\varepsilon^{\infty}_{\alpha\beta}$ in the two phases of lithium niobate. This tensor is related to a second derivative of the electronic energy with respect to an electric field and has been computed using a linear-response technique.[15] All calculations were done using the LDA and no scissors correction has been included. Our results are summarized in Table V, where we also compare the values in the ferroelectric phase to the experiment. The tensors are reported in Cartesian coordinates with the *z* axis along the ferroelectric direction (vector *c* of the hexagonal unit cell, see Sec. III A), the *y* axis in a gliding plane perpendicular to the *a* axis, and *x* along *a*.

The calculated values overestimate the experimental results.[43] This problem has been previously discussed in the literature[44,45] and has been related to the lack of polarization dependence of local and quasilocal exchange-correlation functionals (LDA, GGA). In spite of this error on the absolute value, the evolutions of ε^{∞} are, in general, qualitatively well described by LDA calculations.

TABLE V. Optical dielectric tensors (in Cartesian coordinates) in the two phases of lithium niobate.

Phase		Reference	$\varepsilon^{\infty}_{xx}$	$\varepsilon^{\infty}_{yy}$	$\varepsilon^{\infty}_{zz}$
Paraelectric	Calc.	Present	6.1	6.1	6.9
Ferroelectric	Calc.	Present	5.6	5.6	5.5
	Expt.	60	5.0	5.0	4.6

We first notice that, as observed in related ABO_3 perovskite compounds such as $BaTiO_3$ (Ref. 46) and $KNbO_3$,[47] the amplitude of the dielectric tensor decreases at the transition from the paraelectric to the ferroelectric phase. This can be correlated with the evolution of the band gap. Also, the lowering is strongest along the ferroelectric *z* direction so that the nature of $LiNbO_3$ changes at the transition from positively uniaxial ($\varepsilon^{\infty}_{zz}/\varepsilon^{\infty}_{xx}>1$) to negatively uniaxial ($\varepsilon^{\infty}_{zz}/\varepsilon^{\infty}_{xx}<1$). Another interesting comparison with perovskite compounds concerns the absolute value of ε^{∞}. The amplitude of $\varepsilon^{\infty}_{zz}$ in $LiNbO_3$ is close to what is reported for the cubic and rhombohedral phases of $KNbO_3$ (Ref. 47) (6.63 and 5.49, respectively), while the elements $\varepsilon^{\infty}_{xx}$ and $\varepsilon^{\infty}_{xx}$ are slightly smaller (6.63 and 5.93, repectively, in $KNbO_3$).

B. Born effective charges

The Born effective charges Z^* play a fundamental role in the dynamics of insulating crystal lattices. They govern the amplitude of the long-range Coulomb interaction between nuclei and the splitting between longitudinal (LO) and transverse (TO) optic phonon modes. The Born effective charge tensor of an atom κ is defined as the coefficient of proportionality, at the linear order and under the condition of zero macroscopic electric field, between the macroscopic polarization per unit cell created in the direction β and a cooperative displacement of atoms κ in the direction α,

$$Z^*_{\kappa,\alpha\beta}=\Omega_0\left.\frac{\partial P_\beta}{\partial \tau_{\kappa,\alpha}}\right|_{\mathcal{E}=0}, \tag{1}$$

where Ω_0 is the unit-cell volume. As previously discussed in the literature (see, for instance Ref. 48), Z^* is a dynamical quantity, strongly influenced by dynamical changes of orbital hybridization induced by the atomic displacements. As a consequence, its amplitude is not directly related to that of the static charges and can take anomalous values.

We calculated the Born effective charge tensors in the two phases of $LiNbO_3$ using both the linear-response formalism (LDA calculation) and the Berry phase approach (LDA +GGA calculations). Table VI summarizes the results obtained by linear response for Li_1, Nb_1, and the three O_1, O_2, O_3 oxygen atoms. In the last row, we mention the eigenvalues of the symmetric part of Z^*_O that are identical for all the oxygens. The labels of the atoms correspond to those defined in Sec. III A. The tensors are reported in Cartesian coordinates using the same set of axes as for the dielectric tensor (Sec. IV A).

For comparison, we also determined Z^*_{Nb} using the so-called ''Berry phase approach,'' by approximating Eq. (1) by a finite difference expression

$$Z^*_{\kappa,\alpha\beta}\simeq\Omega_0\frac{\Delta P_\beta}{\Delta \tau_{\kappa,\alpha}}. \tag{2}$$

in which the electronic contribution to the change of polarization is estimated using the same approach as in Sec. III C. To calculate Z^*_{Nb}, we displaced the niobium atom by 0.02 bohr along the three primitive vectors of reciprocal space and

TABLE VI. Born effective charges (in atomic units) of Nb_1, Li_1, O_1, O_2, and O_3 in the two phases of lithium niobate. The last row gives the eigenvalues of the symmetric part of Z_O^* (identical for all the oxygens).

	Paraelectric phase			Ferroelectric phase		
Li_1	1.15	0	0	1.19	−0.25	0
	0	1.15	0	0.25	1.19	0
	0	0	1.11	0	0	1.02
Nb_1	8.28	2.07	0	7.32	1.65	0
	−2.07	8.28	0	−1.65	7.32	0
	0	0	9.17	0	0	6.94
O_1	−1.80	0	0	−1.62	0.31	−0.17
	0	−4.48	2.46	0.23	−4.06	1.79
	0	2.32	−3.43	−0.13	1.85	−2.66
O_2	−3.81	−1.16	−2.13	−3.22	−1.15	−1.46
	−1.16	−2.47	−1.23	−1.23	−2.46	−1.04
	−2.01	−1.16	−3.43	−1.53	−1.04	−2.66
O_3	−3.81	1.16	2.13	−3.68	0.96	1.63
	1.16	−2.47	−1.23	0.88	−2.00	−0.75
	2.01	−1.16	−3.43	1.67	−0.81	−2.66
O Eigenvalues	−6.40	−1.51	−1.80	−5.33	−1.41	−1.60

calculated the polarization difference between this configuration and the equilibrum configuration along these three directions. As in Sec. III C, we used a grid of 20 *k* points in the direction along which we calculated the polarization, and four *k* points in the other two directions. We finally performed a transformation to get the Cartesian components of these tensors. LDA and GGA results are summarized on Table VII.

As expected, within the LDA, the tensors obtained by linear response or using the Berry phase approach are identical within the accuracy of the calculation (± 0.02). However, we note that we had to use a plane-wave kinetic-energy cutoff of 45 hartree to get converged results by linear response, whereas a smaller value of 35 hartree was sufficient using the Berry phase approach. We also observe differences between the LDA and GGA results, the largest one being for the $Z^*_{Nb,33}$ element. In order to get a better insight into the influence of the exchange-correlation functional, we recomputed Z^*_{Nb} in the paraelectric phase using the GGA wave functions but with the geometric parameters (atomic positions and lattice constants) obtained in LDA:

$$Z^*_{Nb} = \begin{pmatrix} 8.30 & 2.08 & 0 \\ -2.08 & 8.30 & 0 \\ 0 & 0 & 9.12 \end{pmatrix}. \quad (3)$$

We observe that the tensor is now very close to that obtained in the LDA. The difference between the results reported in Table VII comes, therefore, principally from the fact that LDA and GGA give slightly different geometrical parameters, whereas the Berry phase itself is quite insensitive to the approximation used for the exchange-correlation energy.

Analyzing now the charges reported in Table VI, we observe that Z^*_{Li} is nearly isotropic and that the diagonal elements have a value close to the nominal charge of the lithium atom $(+1)$. On the other hand, the amplitude of Z^*_{Nb} is highly *anomalous* in the sense that it is significantly larger than the nominal charge expected in a purely ionic crystal $(+5)$. The niobium charge is slightly anisotropic with a significantly different value along the trigonal axis. For the oxygen atoms, the anisotropy is much stronger. This feature appears clearly from the inspection of the tensor eigenvalues. The highest eigenvalue is strongly *anomalous* (-6.4 for the paraelectric phase, compared to the nominal charge of -2) and the inspection of the associated eigenvector reveals that it is the charge associated with an oxygen displacement (nearly) along the Nb-O bond. In contrast, the two other eigenvalues (associated with oxygen displacement in the plane perpendicular to the Nb-O bond) are smaller than -2.

Most of our observations on $LiNbO_3$ are comparable to what has been previously reported for related perovskite compounds such as $KNbO_3$ (Refs. 41 and 47) or $NaNbO_3$.[41] For instance, the Nb charge in the paraelectric phase for a displacement along the Nb-O bond is, respectively, equal to 8.75, 9.11, and 9.23 in $LiNbO_3$, $NaNbO_3$,[41] and $KNbO_3$,[41] while the Li, Na, and K charges are equal, respectively, to 1.11, 1.13, and 1.14.

The amplitude of the charge in $LiNbO_3$ can be explained following the same line of thought as Ghosez *et al.* for perovskite compounds in Ref. 48. The Li atom is close to a fully ionized configuration and only carries its nominal charge. On the other hand, there is a partly covalent interaction between Nb and O, which is responsible for their *anomalous* effective charges and for the strong anisotropy of the oxygen tensor, as is made plausible within the bond orbital model of Harisson.[49] During an atomic displacement, the parameters that determine the covalent interactions between the Nb $4d$ and O $2p$ atomic orbitals (the hopping integrals) vary. This variation produces a dynamical charge transfer between the niobium and the oxygen atoms, which is at the origin of the anomalous part of Z^*_{Nb} and Z^*_O.

TABLE VII. Born effective charges of the niobium atom calculated using the Berry phase approach in LDA and GGA.

	Paraelectric phase			Ferroelectric phase		
LDA	8.26	2.07	0	7.30	1.61	0
	−2.07	8.26	0	−1.61	7.30	0
	0	0	9.08	0	0	6.83
GGA	8.40	2.10	0	7.23	1.59	0
	−2.10	8.40	0	−1.59	7.23	0
	0	0	9.29	0	0	6.46

TABLE VIII. Band-by-band decomposition of the Born effective charge of the niobium atom (LDA calculation).

Bands	Nominal	Paraelectric phase			Ferroelectric phase		
Z_{core}	13.00	13.00	0	0	13.00	0	0
		0	13.00	0	0	13.00	0
		0	0	13.00	0	0	13.00
Nb 4s	−2.00	−2.04	0.03	0.00	−2.06	0.02	0.00
		−0.03	−2.04	0.00	−0.02	−2.06	0.00
		0.00	0.00	−2.02	0.00	0.00	−2.04
Li 1s	0.00	0.01	−0.01	0.00	0.01	−0.00	0.00
		0.01	0.01	0.00	0.00	0.01	0.00
		0.00	0.00	0.00	0.00	0.00	0.00
Nb 4p	−6.00	−6.42	−0.06	0.00	−6.49	−0.05	0.00
		0.06	−6.42	0.00	0.05	−6.49	0.00
		0.00	0.00	−6.37	0.00	0.00	−6.35
O 2s	0.00	0.57	0.09	0.00	0.60	0.10	0.00
		−0.09	0.57	0.00	−0.10	0.60	0.00
		0.00	0.00	0.58	0.00	0.00	0.50
O 2p	0.00	3.14	1.89	0.00	2.25	1.45	0.00
		−1.89	3.14	0.00	−1.45	2.25	0.00
		0.00	0.00	3.89	0.00	0.00	1.71
Total	5.00	8.26	2.07	0.00	7.30	1.62	0.00
		−2.07	8.26	0.00	−1.62	7.30	0.00
		0.00	0.00	9.08	0.00	0.00	6.83

The essential role played by the O 2p bands can be emphasized from the analysis of the contribution of the different isolated sets of bands (as identified in Fig. 2) to the global niobium charge. Individual contributions were obtained thanks to formula (16) of Ref. 36 by considering only the Bloch functions associated with a particular set of bands as elements of the overlap matrix. The results of the decomposition are summarized in Table VIII. The first line (Z_{core}) brings together the nucleus and core electron contributions. The last row corresponds to the total charge. The second column refers to the isotropic nominal value that would be expected in a purely ionic compound. All the deviations with respect to this reference *isotropic* nominal value are referred to as *anomalous*.

Focusing first on the deep Nb 4s and Li 1s levels, we do not identify any significant anomalous contribution, in agreement with the fact that these electrons do not participate in the bonding. On the contrary, the anomalous O 2p contribution is very large and mainly responsible for the total anomalous charge. This can be explained by dynamical changes of the Nb 4d orbital contribution to the O 2p bands producing a dynamical transfer of electrons from O to Nb when the Nb-O distance shortens. We note finally small and compensating anomalous contributions at the level of the Nb 4p and O 2s bands: they reveal the existence of hybridizations between these levels.

If we now compare the result in the paraelectric and in the ferroelectric phases in Table VI, we observe a global decrease of the charges in the ferroelectric state, especially along the ferroelectric direction. This is similar to what has been reported for the perovskite compounds. If we look at Table VIII, we see that for Z^*_{Nb} this reduction originates in a modification of the O 2p contribution only. It confirms the strong influence of the phase transition on the O 2p–Nb 4d hybridizations as discussed in Sec. III B. All the other contributions remain unaffected confirming that only the O 2p bands are affected by the phase transition.

In Sec. III C, we had computed the spontaneous polarization of lithium niobate by using the Berry phase formulation proposed by King-Smith and Vanderbilt. From the tensors reported in Table VI, one can also obtain a rough estimate of the spontaneous polarization by using the following formula:

$$P_{s,\alpha}=\frac{1}{\Omega_0}\sum_{\kappa,\beta} Z^*_{\kappa,\alpha\beta}\delta\tau_{\kappa,\beta}, \tag{4}$$

where $\delta\tau_{\kappa,\beta}$ represents the displacement of atom κ during the phase transition. The calculation can be performed using the atomic positions reported in Sec. III A and keeping the lattice constants of the paraelectric phase. We obtain a value of 0.83 C/m^2 and 0.67 C/m^2 by using, respectively, the effective charges of the paraelectric and ferroelectric phases. At first, this illustrates that the reduction of Z^* has a strong effect on the magnitude of P_s. Moreover, comparing these values to those reported in Table IV, we see that the spontaneous polarization is not the mean of the two values estimated from the effective charges: this points out that the evolution of the charges along the ferroelectric path of atomic displacement is highly *nonlinear*. A similar behavior was observed for barium titanate.[48]

V. PHONONS AT THE Γ POINT

A. Paraelectric phase

The paraelectric phase belongs to the space group $R\bar{3}c$. At the Γ point, the optical-phonon modes can be classified according to its irreductible representations into

$$A_{1g}\oplus 2A_{1u}\oplus 3A_{2g}\oplus 3A_{2u}\oplus 4E_g\oplus 5E_u\,.$$

The A_{2u} and E_u modes are infrared active. At the Γ point, they are split into transverse and longitudinal components A^T_{2u} (E^T_u) and A^L_{2u} (E^L_u). This splitting can be calculated from the Born effective charges and the optical dielectric tensor (see Sec. IV A), as described in Ref. 15.

The frequencies of the transverse and longitudinal modes are listed in Table IX. As no experimental data are available, we only compare our results to the frequencies calculated by Parlinski *et al.*[11] Both calculations identify unstable A_{2u} and A_{2g} modes. Our calculated frequencies are mostly in reasonable agreement with those of Parlinsky *et al.*, but there are exceptions, as for the E_g mode at 501 cm^{-1}. That could eventually be explained by strong anharmonicities of the potential energy to which our method is less sensitive. Another major difference is that the lowest E^T_u mode is unstable in our

TABLE IX. Phonon frequencies (in cm^{-1}) of the transverse and longitudinal modes in the paraelectric phase of lithium niobate.

Silent modes			Infrared active modes				
	Present	Ref. 11		Present	Ref. 11		Present
A_{1g}	403	415	A_{2u}^T	201i	227i	A_{2u}^L	90i
A_{1u}	279	294		94	116		346
	435	481		478	520		838
A_{2g}	115i	151i					
	405	393	E_u^T	53i	77	E_u^L	174
	889	912		177	152		274
E_g	175	162		393	411		419
	425	433		460	539		508
	501	617		532	614		844
	589	644					

calculation, whereas Parlinski *et al.* identify it as stable. The frequency of this mode is low, so that it is probably very sensitive to numerical errors. Anticipating what is discussed at the end of this section, we note that the instability of this mode is related to its giant effective charge and is, therefore, plausible.

At first, we note that it is the most unstable A_{2u}^T mode that drives the paraelectric to ferroelectric phase transition. The dynamical matrix eigenvectors associated with this mode is

$$\mathrm{Li}_1(0,0,0.466),$$

$$\mathrm{Nb}_1(0,0,0.216),$$

$$\mathrm{O}_1(0,-0.050,-0.276),$$

$$\mathrm{O}_2(0.043,0.025,-0.276),$$

$$\mathrm{O}_3(-0.043,0.025,-0.276).$$

It is worth noticing that it has an overlap of 0.99 with the vector representing the atomic displacements during the phase transition (for which we have chosen the same normalization as for the phonon eigenvectors).

To have a better insight into the microscopic origin of the different instabilities, we can use a model already applied by Ghosez *et al.*[46] to explain the phonon instability in barium titanate, which is based on a seminal idea of Cochran.[50] The interatomic forces in a crystal can be decomposed into short-range forces and long-range Coulomb (dipole-dipole) interactions. A structural instability can appear from the cancellation of both contributions.

By following the notations of Ref. 46, we can write the full dynamical matrix A as the sum of a contribution due to the short-range forces (A_{SR}) and a contribution due to the dipole-dipole interactions (A_{DD}). The latter one can be evaluated by using Ewald summation techniques, as is described in Ref. 51, whereas A_{SR} is obtained by subtracting A_{DD} from the full dynamical matrix A. Using this approach, we can decompose ω^2 as the sum of two contributions ω_{DD}^2 and ω_{SR}^2:

TABLE X. DD and SR contributions to the TO mode frequency squared (cm^{-2}) for the soft modes in the paraelectric phase.

	A_{2u}^T (201i)	A_{2g} (115i)	E_u^T (53i)
ω_{DD}^2	−88803	109023	−298387
ω_{SR}^2	48260	−122248	295571
ω^2	−40543	−13225	−2816

$$\underbrace{\langle \eta|A|\eta\rangle}_{\omega^2} = \underbrace{\langle \eta|A_{SR}|\eta\rangle}_{\omega_{SR}^2} + \underbrace{\langle \eta|A_{DD}|\eta\rangle}_{\omega_{DD}^2}, \tag{5}$$

where η is an eigenvector of the full dynamical matrix. Table X gives the results of this decomposition for the three unstable modes of the paraelectric phase.

The A_{2u}^T mode that drives the phase transition is strongly destabilized by the dipole-dipole interactions that are not fully compensated by the short-range forces, which tend to stabilize the paraelectric structure. The large amplitude of the dipolar interaction must be related to the high mode effective charge equal to 6.71.[54] Similarly, the E_u^T mode at 53i cm^{-1} is strongly destabilized by the dipole-dipole interactions as we could expect from its even larger mode effective charge equal to 9.78. It is interesting to note that the square of its frequency is the sum of two very large terms that nearly cancel so that the resultant frequency is quite small.

B. Ferroelectric phase

At the Γ point, the optical phonons can be classified according to the irreductible representations of the space group $R3c$ into

$$4A_1 \oplus 5A_2 \oplus 9E.$$

The A_1 and E modes are Raman and infrared active so that they are split into transverse and longitudinal components.

1. A modes

Tables XI and XII summarize the frequencies of the transverse and longitudinal A_1 modes that we have computed. Our results are compared to the frequencies calculated by Parlinski *et al.*[11] and Caciuc *et al.*[10] and to the experimental frequencies obtained by Raman and infrared spectroscopy. We note that the longitudinal frequencies reported by Parlin-

TABLE XI. Phonon frequencies (in cm^{-1}) of the four transverse A_1 modes in the ferroelectric phase.

Calc. frequencies			Expt. frequencies		
Present	Ref. 10	Ref. 11	Ref. 52	Ref. 53	Ref. 60
243	208	239	252	251	252
288	279	320	275	273	276
355	344	381	332	331	333
617	583	607	632	631	634

TABLE XII. Phonon frequencies (in cm^{-1}) of the four longitudinal A_1 modes in the ferroelectric phase.

Calc. frequencies		Expt. frequencies		
Present	Ref. 11	Ref. 60	Ref. 59	Ref. 61
287	309	273	275	273
348	381	306	333	332
413	548	423	436	436
855	831	869	876	873

ski *et al.* were obtained using an empirical guess of the Born effective charges and the optical dielectric tensor. The longitudinal modes have their wave vector along the *z* axis while the wave vectors of the transverse modes are perpendicular to it.

The calculated and measured frequencies of the A_2 modes are summarized in Table XIII. Experimental data comes from inelastic neutron scattering.[55] Our results are quite close to the experimental data. They present, in general, a similar error as those obtained in previous calculations.

The A_1 mode at 234 cm^{-1} has the strongest overlap (0.82) with the A_{2u} mode that drives the phase transition in the paraelectric phase. By analyzing the interatomic forces for this mode, we found $\omega_{DD}^2 = -67\,649$ cm^{-2} and $\omega_{SR}^2 = 126\,618$ cm^{-2}, respectively. This helps us to clarify the stabilization of the soft mode after the phase transition. Although the Born effective charges decrease at the transition, the dipole-dipole interactions remain quite strong in the ferroelectric phase (strong enough to destabilize the mode in the paraelectric phase), and it is the increase of the short-range forces that stabilizes this mode. This behavior contrasts with what was observed in barium titanate,[46] where it is a decrease of the dipole-dipole interactions that stabilizes the ferroelectric mode in the rhombohedral phase.

2. E modes

The analysis of the nine *E* modes is more difficult. In the literature, many different frequencies have been reported, which where differently assigned. This comes from the fact that the properties of lithium niobate crystals strongly depend on the internal and external defects.[6] In particular, Raman spectroscopy is very sensitive to small modifications in the structure and to the stoichiometry of the samples.[56,57]

For the transverse optic phonons, most authors seem to agree on seven modes around 152, 237, 265, 322, 368, 431, and 580 cm^{-1}. For the two missing modes, Ridah *et al.*[56] and Repelin *et al.*[57] suggest frequencies at 180 and 610 cm^{-1}, Kaminow and Johnston[58] report modes at 92 and 630 cm^{-1} and Claus *et al.*[59] mention phonons at 668 and 743 cm^{-1}. Barker and Loudon[60] were tempted to identify the modes at 180 and 610 cm^{-1} for mixed phonons that have their wave vector at 45° from the *z* axis and the mode at 670 cm^{-1} for a combination band. Yang *et al.*[61] report modes at 152 and 530 cm^{-1} and suggest that the frequencies at 741 and 667 cm^{-1} are due to combination bands.

TABLE XIII. Phonon frequencies (in cm^{-1}) of the A_2 modes in the ferroelectric phase.

Calc. frequencies			Expt. frequency
Present	Ref. 10	Ref. 11	Ref. 55
218	153	220	224
297	287	321	314
412	417	432	
454	439	462	455
892	883	893	

For the transverse *E* modes, all the experimental values mentioned above as well as the theoretical results of Caciuc *et al.*[10] and Parlinski *et al.*[11] are summarized in Table XIV, while the frequencies of the longitudinal *E* modes are given in Table XV.

One can see that there are some discrepancies between the frequencies reported by the various authors. Even the previous first-principles calculations do not clarify all ambiguities. Parlinski *et al.*, whose results are relatively similar to ours, assign the seven modes reported by most authors as well as phonons at 423 and 690 cm^{-1}, while Caciuc *et al.* suggest the existence of phonons at 167 and 617 cm^{-1}, as was proposed by Ridah *et al.* and Repelin *et al.* In order to clarify the identification of the *E* modes, we will analyze two quantities related to the phonon modes that have been measured experimentally in the past: the directional dispersion branches of the extraordinary phonons (Fig. 3) and the mode oscillator strengths (Table XVI).

Figure 3 shows the dependence of the phonon frequencies on the angle θ between the *c* axis and the phonon wavevector $\mathbf{q}$ in the limit of long wavelengths ($\mathbf{q} \rightarrow 0$). This calculated directional dispersion relation agrees with the experimental measurements of Refs. 59 and 61 for the branches (1)–(5) and (8)–(13). One main difference is the absence of branch (7) in both works and the fact that they report a different behavior for branch (6): according to their results, the A_{1L} mode transforms into an A_{1T} mode and not into an E_L mode as we have observed. This discrepancy is probably due to the fact that our calculation slightly overestimates the frequency of the corresponding A_{1T} mode and predicts a frequency larger than that of the E_L mode, while experimentally the inverse has been found. Further differences concern branches at 743 cm^{-1} (Ref. 59) and 152 and 530 cm^{-1} (Ref. 61) that are not reproduced by our calculation and that have not been found in the other experimental studies. We can assume that they are not related to first-order phonons.

On the basis of Fig. 3 we will now discuss the assignation of selected phonon modes in Tables XIV and XV. Ridah *et al.* and Repelin *et al.* report an E_T mode at 180 cm^{-1} that has also been found by Caciuc *et al.* but not by Parlinski *et al.* and neither in our study. As mentioned before, Barker *et al.* associate this frequency to a mixed phonon with the wave vector at 45° with the *z* axis. By looking at the spectra reported in the papers of Ridah *et al.* and Repelin *et al.* (Fig. 3 of Ref. 56 and Fig. 2(b) of Ref. 57), we see that this mode has indeed its wave vector in this direction [Ridah *et al.*, for example, measure it only in an $X(ZY)Z$ orientation, which allows them to detect transverse *E* modes, whose wave vec-

TABLE XIV. Phonon frequencies (in cm^{-1}) of transverse E modes in the ferroelectric phase.

Calc. frequencies			Expt. frequencies						
Present	Ref. 10	Ref. 11	Ref. 56	Ref. 57	Ref. 58	Ref. 59	Ref. 60		Ref. 61
					92				
155	151	157	153	155	152	155	152	152	152[a]
	167		177	180					
218	236	214	238	238	238	238	236	238	236
264		269	264	265	262	265	265	264	263
330	307	349	322	325	322	325	322	321	322
	334								
372	352	419	369		368		363	367	
384		423		371	371		370		
428	432	446	432	431	436	431	431	434	431
									530
585	526	605	580	582	582	582	586	579	578
	617		610	610					
					630				
677		690				668	670		
						743			

[a]The authors of Ref. 61 suggest that there are two different E_T modes at 152 cm^{-1}.

tors form an angle of 45° with the z axis]. One can see from Fig. 3 that the E_T mode at 155 cm^{-1} [branch (1)] transforms smoothly into the E_L mode at 197 cm^{-1} when θ varies from 0° to 90°. At 45°, the frequency of this mode is 174 cm^{-1} and it has a strong transverse component [$\mathbf{q}$ is along the direction (0,1,1)] as one can see it from its mode effective charge

$$(0,-2.92,2.35).$$

Therefore, we believe that Ridah *et al.* and Repelin *et al.* have measured this particular mode and we propose that the second pure transverse E mode has in fact a frequency of 234 cm^{-1}, in agreement with the results of Parlinski *et al.* We should note that we observe a similar behavior for branch (11): the E_T mode at 585 cm^{-1} gives rise to a mode of 601 cm^{-1} for $\theta=45°$. As Barker *et al.*, we are, therefore, tempted to assign the reported frequencies around 610 cm^{-1} to such a kind of mixed phonon and not to a pure transverse mode.[62]

TABLE XV. Phonon frequencies (in cm^{-1}) of longitudinal E modes in the ferroelectric phase.

Calc. frequencies		Expt. frequencies			
Present	Ref. 11	Ref. 60	Ref. 59	Ref. 61	Ref. 56
				152	186
197	204	198	198	194	195
224	216	238	243	240	240
298	316	296	295	295	299
349	372	342			345
384	422		371	370	
423	445	418	428	425	424
452	570	450	454	460	456
				530	
					625
675	677	660	668		
			739		
863	856	878	880	878	878

One can see also from Table XIV that Caciuc *et al.* do not associate the measured mode at 264 cm^{-1} to any of their calculated phonons in spite of the fact that it has been observed in all the experiments cited above. They suggest that the measured line is due to a breaking of the Raman selection rules caused by anharmonic effects and that it corresponds to the lowest A_{1T} mode. Their main argument is that Claus *et al.* have observed that this E_T mode transforms into the mentioned A_{1T} mode as θ varies from 0° to 90°. On the other hand (but in agreement with Parlinski *et al.*), we reproduce in our calculation a mode at 264 cm^{-1} of E symmetry. Moreover, as illustrated in Fig. 3, this mode exhibits an angular disipersion [branch (3)] similar to that experimentally measured by Claus *et al.* This gives us a strong argument to propose that the measured mode at 264 cm^{-1} is a real E-mode.

The last point we would like to discuss related to Fig. 3 concerns the E_T modes at 372 and 384 cm^{-1}. In Table XIV, they were associated with measured frequencies at 369 and 371 cm^{-1} that we believe to be related to two different phonons in spite of the fact that all the other authors associate them to the same. This is in fact already plausible from a careful analysis of the existing experimental data: The E_T and E_L modes at 384 cm^{-1} in Tables XIV and XV correspond to branch (8) in Fig. 3. This branch has been measured by Claus *et al.* and Yang *et al.* while line (7) is absent in both works. Now, it is interesting to note that Ridah *et al.* and Barker *et al.* report a couple of E_T-E_L modes at 369 and 342 cm^{-1} that have not been reported by Claus *et al.* and Yand *et al.*, but that we believe to be related to line (7). This

observation suggests that the measured frequencies of 369 and 371 cm^{-1} correspond to two different first-order E_T modes that cannot be distinguished in the spectra due to the small difference in their frequencies.

A considerably stronger certification of the existence of two phonons arround 370 cm^{-1} can be obtained from the inspection of Table XVI, where we compare the mode-oscillator strengths to the experimental values measured by Barker *et al.* The mode-oscillator strength $S_{m,\alpha\beta}$ for mode m was calculated from the Born effective charges and the phonon eigenvectors according to the relation

$$S_{m,\alpha\beta}=\left(\sum_{\kappa,\gamma} Z^*_{\kappa,\gamma\alpha}\eta^{(m)}(\kappa,\gamma)\right)\left(\sum_{\kappa,\gamma} Z^*_{\kappa,\gamma\beta}\eta^{(m)}(\kappa,\gamma)\right). \tag{6}$$

For the A_1 modes, the agreement is reasonable. For most E modes, the agreement with experiment is much better except for the last mode. The table shows, in particular, that the assumption concerning the E modes at 369 (372) and 371(384) cm^{-1} is reasonable: Barker *et al.* report a mode-oscillator strength of 3.59 for the mode at 369 cm^{-1}, in agreement with what we found for the mode at 372 cm^{-1}. The fact that they did not observe the mode at 371 cm^{-1} in their infrared measurements can also easily be understood as originating in its small mode-oscillator strength.

On the contrary, Yang *et al.* as well as Claus *et al.* measured a mode at 371 cm^{-1} for which they report a frequency that does not vary with θ. If this frequency was related to the phonon measured by Barker *et al.*, the mode oscillator strength of 3.59 would give rise to a measurable angular dependence. The abscence of angular dispersion is, therefore, the proof that it must correspond to another phonon with a negligible oscillator strength, as our mode at 384 cm^{-1} associated with line (8) in Fig. 3.

Let us conclude this section by mentioning that the isotopic effect $^7Li \rightarrow {}^6Li$ on the phonon frequencies has been recently investigated by Repelin *et al.*[57] For the mode at 371 cm^{-1}, they measured a shift of 17 cm^{-1}. For the mode at 372 cm^{-1} and 384 cm^{-1} our calculations reproduce a shift of 22 cm^{-1} and 23 cm^{-1}, respectively. These two values are comparable to what has been measured. Moreover, the similar shift of the two modes justifies why no splitting has been identified for these two nearly degenerated modes during the isotopic effect experiment.

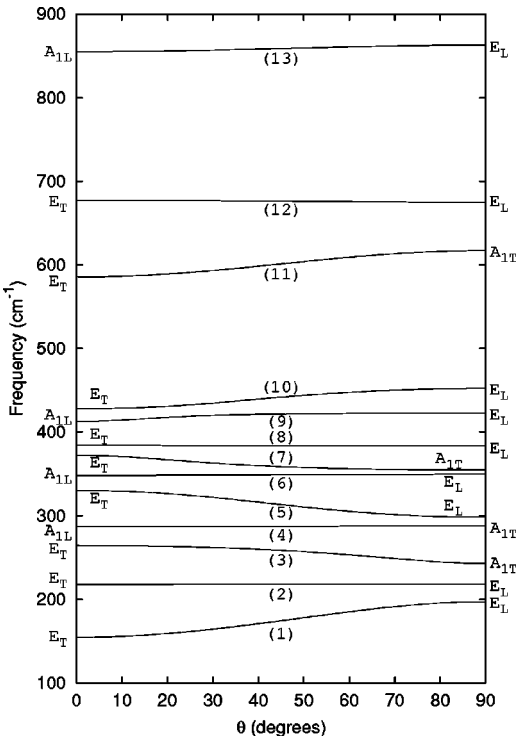

FIG. 3. Directional dispersion branches of extraordinary phonons in the ferroelectric phase of $LiNbO_3$. θ is the angle between the c axis and the phonon wave vector **q**.

3. Static dielectric tensor

In Sec. IV A, we have reported the optical dielectric tensor $\varepsilon^{\infty}_{\alpha\beta}$. This quantity describes the response of the electron gas to a homogenous electric field if the ions are taken as fixed at their equilibrum positions. To include the response of the crystal lattice to the electric field, one can use a model that assimilates the solid to a system of undamped harmonic oscillators,[15]

$$\varepsilon^0_{\alpha\beta}=\varepsilon_{\alpha\beta}(\infty)+\frac{4\pi}{\Omega_0}\sum_m \frac{S_{m,\alpha\beta}}{\omega_m^2}. \tag{7}$$

TABLE XVI. Mode-oscillator strengths (in 10^{-4} atomic units) of the active modes in the ferroelectric phase of lithium niobate. For each mode, we also recall the calculated frequency.

A_1 modes			E modes		
Freq.	S_m, Calc.	S_m, Expt. (Ref. 60)	Freq.	S_m, Calc	S_m, Expt. (Ref. 60)
243	13.29	11.66	155	5.89	6.02
288	0.20	0.89	218	0.55	0.53
355	0.45	0.18	264	4.38	4.58
617	14.57	11.92	330	2.71	2.70
			372	3.59	3.59
			384	0.15	
			428	0.31	0.40
			585	14.33	13.43
			677	0.37	1.06

TABLE XVII. Static dielectric tensor in the ferroelectric phase of lithium niobate.

	Reference	ε^0_{xx}	ε^0_{yy}	ε^0_{zz}
Calc.	Present	42.4	42.4	29.3
Expt.	60	41.5	41.5	26.0
Expt.	61	43.6	43.6	24.3

The calculated and measured elements of $\varepsilon^0_{\alpha\beta}$ are summarized in Table XVII. The agreement is very good for the elements ε^0_{xx} and ε^0_{yy}, while ε^0_{zz} overestimates the experimental value. This result was predictable because we saw in the preceding section that the calculated mode-oscillator strengths agree better for the E modes than for the A_1 modes.

Looking back at Table XVI, we observe that the two A_1 modes at 243 and 617 cm^{-1} have a large oscillator strength. However, due to their different frequency they do not contribute equally to ε^0_{zz}: the main contribution (84%) comes from the A_1 mode at 243 cm^{-1}, while only 14% are originating from the mode at 617 cm^{-1}. For ε^0_{xx} and ε^0_{yy} we do not observe such a clear domination of one mode. The most important contributions come from the modes at 155 cm^{-1} (59%), 264 cm^{-1} (15%) and 585 cm^{-1} (10%).

VI. CONCLUSIONS

Using a plane-wave pseudopotential approach to density-functional theory, we studied structural, electronic, dielectric, and dynamical properties of the two phases of lithium niobate. In particular, the amplitude of the optical dielectric tensor and of the Born effective charges have been obtained.

Some of our results were computed within the LDA and GGA for the exchange-correlation energy. We found that the use of the GGA has only a small influence on quantities such as the Born effective charges or the spontaneous polarization, while it has a stronger impact on the optimized lattice parameters and atomic positions.

The analysis of the Born effective charges revealed several features that have already been observed in similar studies performed on perovskite oxides: Z^*_{Nb} as well as Z^*_{O} are larger than their nominal ionic charge while Z^*_{Li} is rather close to it. The first two tensors decrease during the transition from the paraelectric to the ferroelectric phase, while the latter one remains quite constant. All these results could be explained from the mixed ionic/covalent character of the chemical bonds in lithium niobate, especially from the partial hybridization between Nb $4d$ and O $2p$ states.

By examining the zone-center phonons in the paraelectric phase, we have shown that a soft A_{2u} mode is responsible for the ferroelectric transition, and from a model calculation we identified the destabilizing long-range dipolar forces to be at the origin of this phonon instability. During the discussion of the phonons in the ferroelectric phase, we paid much attention to the identification of the E modes. We tried to clarify the remaining ambiguities and proposed an assignation justified by the analysis of the mode-oscillator strengths and the angular dispersion relation of the extraordinary phonons.

ACKNOWLEDGMENTS

M.V. is grateful to the National Fund for Scientific Research (FNRS, Belgium). Ph.G. acknowledges support from FNRS, Belgium (Grant No. 9.4539.00) and the Université deLiège (Impulsion grant). This work was supported by the Volkswagen-Stiftung (www.volkswagenstiftung.de) within the program ''Complex Materials: Cooperative Projects of the Natural, Engineering, and Biosciences'' with the title ''Nano-sized ferroelectric Hybrids,'' under Project No. I/77 737.

[1] M. E. Lines and A. M. Glass, *Principles and Applications of Ferroelectrics and Related Materials* (Clarendon Press, Oxford, 1977).

[2] H. Nishihara, M. Haruna, and T. Suhara, in *Optical Integrated Circuits*, edited by R. E. Fischer and W. J. Smith, Optical and Electro-Optical Engineering Series (Mcgraw-Hill, New York, 1985).

[3] L. Wooten, K.M. Kissa, A. Yi-Yan, E.J. Murphy, D.A. Lafaw, P.F. Hallemeier, D. Maack, D.V. Attanasio, D.J. Fritz, G.J. McBrien, and D.E. Bossi, IEEE J. Sel. Top. Quantum Electron. **6**, 69 (2000).

[4] K. Buse, A. Adibi, and D. Psalti, Nature (London) **393**, 665 (1998).

[5] L. Hesselink, S.S. Orlov, A. Liu, A. Akella, D. Lande, and R.R. Neurgaonkar, Science **282**, 1089 (1998).

[6] A. Räuber, in *Current Topics in Materials Science*, edited by E. Kaldis (North-Holland, Amsterdam, 1978), Vol. 1, p. 481.

[7] I. Inbar and R.E. Cohen, Phys. Rev. B **53**, 1193 (1996).

[8] I. Inbar and R.E. Cohen, Ferroelectrics **194**, 83 (1997).

[9] A.V. Postnikov, V. Caciuc, and G. Borstel, J. Phys. Chem. Solids **61**, 295 (2000).

[10] V. Caciuc, A.V. Postnikov, and G. Borstel, Phys. Rev. B **61**, 8806 (2000).

[11] K. Parlinski, Z.Q. Li, and Y. Kawazoe, Phys. Rev. B **61**, 272 (2000).

[12] P. Hohenberg and W. Kohn, Phys. Rev. **136**, B864 (1964).

[13] W. Kohn and L.J. Sham, Phys. Rev. **140**, A1133 (1965).

[14] ABINIT is a common project of the Université Catholique de Louvain, Corning Incorporated, and other contributors (http://www.pcpm.uc l. ac.be/abinit).

[15] X. Gonze and C. Lee, Phys. Rev. B **55**, 10 355 (1997).

[16] X. Gonze, Phys. Rev. B **55**, 10 337 (1997).

[17] S. Goedecker, SIAM J. Sci. Comput. (USA) **18**, 1605 (1997).

[18] M.C. Payne, M.P. Teter, D.C. Allan, T.A. Arias, and J.D. Joannopoulos, Rev. Mod. Phys. **64**, 1045 (1992).

[19] X. Gonze, Phys. Rev. B **54**, 4383 (1996).

[20] J.P. Perdew and Y. Wang, Phys. Rev. B **45**, 13 244 (1992).

[21] J.P. Perdew, K. Burke, and M. Ernzerhof, Phys. Rev. Lett. **77**, 3865 (1996).

[22] N. Troullier and J.L. Martins, Phys. Rev. B **43**, 1993 (1991).
[23] M. Fuchs and M. Scheffler, Comput. Phys. Commun. **119**, 67 (1999).
[24] H.J. Monkhorst and J.D. Pack, Phys. Rev. B **13**, 5188 (1976).
[25] H. Boysen and F. Altorfer, Acta Crystallogr., Sect. B: Struct. Sci. **B50**, 405 (1994).
[26] J. Goniakowski, J.M. Holender, L.N. Kantorovich, M.J. Gillan, and J.A. White, Phys. Rev. B **53**, 957 (1996).
[27] C. Filippi, D.J. Singh, and C.J. Umrigar, Phys. Rev. B **50**, 14 947 (1994).
[28] G. F. Koster, in *Solid State Physics*, edited by F. Seitz and D. Turnball (Academic, New York, 1957), p. 173.
[29] Ph. Ghosez, X. Gonze, and J.-P. Michenaud, Ferroelectrics **220**, 1 (1999).
[30] R.D. King-Smith and D. Vanderbilt, Phys. Rev. B **49**, 5828 (1994).
[31] R.E. Cohen, Nature (London) **358**, 136 (1992).
[32] R.E. Cohen and H. Krakauer, Ferroelectrics **136**, 65 (1992).
[33] R.O. Jones, and O. Gunnarson, Rev. Mod. Phys. **61**, 689 (1989).
[34] A. Dhar and A. Mansingh, J. Appl. Phys. **68**, 5804 (1990).
[35] R. Resta, Rev. Mod. Phys. **66**, 899 (1994).
[36] R.D. King-Smith and D. Vanderbilt, Phys. Rev. B **47**, 1651 (1993).
[37] D. Vanderbilt and R.D. King-Smith, Phys. Rev. B **48**, 4442 (1993).
[38] S.H. Wemple, M. DiDomenico, Jr., and I. Camlibel, Appl. Phys. Lett. **12**, 209 (1968).
[39] A.M. Glass and M.E. Lines, Phys. Rev. B **13**, 180 (1976).
[40] L. Hafid and F.M. Michel-Calendini, J. Phys. C **19**, 2907 (1986).
[41] W. Zhong, R.D. King-Smith, and D. Vanderbilt, Phys. Rev. Lett. **72**, 3618 (1994).
[42] X. Gonze, Ph. Ghosez, and R.W. Godby, Phys. Rev. Lett. **78**, 294 (1997).
[43] The overestimate (10%) is smaller than that usually observed for perovskite ABO_3 compounds (20%).This can be related to the smaller discrepancy obtained for the electronic band gap in the case of $LiNbO_3$.
[44] X. Gonze, Ph. Ghosez, and R.W. Godby, Phys. Rev. Lett. **74**, 4035 (1995).
[45] Ph. Ghosez, X. Gonze, and R.W. Godby, Phys. Rev. B **56**, 12 811 (1997).
[46] Ph. Ghosez, X. Gonze, and J.-P. Michenaud, Europhys. Lett. **33**, 713 (1996).
[47] C.Z. Wang, R. Yu, and H. Krakauer, Phys. Rev. B **54**, 11 161 (1996).
[48] Ph. Ghosez, J.-P. Michenaud, and X. Gonze, Phys. Rev. B **58**, 6224 (1998).
[49] W. A. Harrison, *Electronic Structure, and the Properties of Solids* (Freeman San Francisco, 1980).
[50] W. Cochran, Adv. Phys. **9**, 387 (1960).
[51] X. Gonze, J.C. Charlier, D.C. Allan, and M.P. Teter, Phys. Rev. B **50**, 13 035 (1994).
[52] A. Ridah, M.D. Fontana, and P. Bourson, Phys. Rev. B **56**, 5967 (1997).
[53] U.T. Schwarz and M. Maier, Phys. Rev. B **55**, 11 041 (1997).
[54] For the mode effective charge Z_m^*, we use the same conventions as used by the authors of Ref. 15:
$$Z^*_{m,\beta}=\left(\sum_{\kappa,\alpha} Z^*_{\kappa,\alpha\beta}\eta^{(m)}_{\mathbf{q}=0}(\kappa,\alpha)\right)\Bigg/\left(\sqrt{\sum_{\kappa,\alpha}[\eta^{(m)}_{\mathbf{q}=0}(\kappa,\alpha)]^2}\right).$$
[55] M.R. Chowdhury, G.E. Peckham, and D.H. Saunderson, J. Phys. C **11**, 1671 (1978).
[56] A. Ridah, P. Bourson, M.D. Fontana, and G. Malovichko, J. Phys.: Condens. Matter **9**, 9687 (1997).
[57] Y. Repelin, E. Husson, F. Bennani, and C. Proust, J. Phys. Chem. Solids **60**, 819 (1999).
[58] I.P. Kaminow and W.D. Johnston, Jr., Phys. Rev. **160**, 519 (1967).
[59] R. Claus, G. Borstel, E. Wiesendanger, and L. Steffan, Z. Naturforsch. A **27A**, 1187 (1972).
[60] A.S. Barker, Jr. and R. Loudon, Phys. Rev. **158**, 433 (1967).
[61] X. Yang, G. Lan, B. Li, and H. Wang, Phys. Status Solidi B **142**, 287 (1987).
[62] For the sake of completeness, we should mention that this mode has not only been observed in an $X()Z$ configuration as is the case for the mode at 180 cm^{-1}, but also in an $X()Y$ configuration, which allows to measure phonons whose wave vectors are in the plane perpendicular to the c axis. This argument, thus, holds less than for the mode at 180 cm^{-1}.